Amplitude and Phase Estimation of Real - Valued Sine-wave Via Frequency-Domain Linear Least-Squares Algorithms

Daniel Belega[1], *Member, IEEE,* Dario Petri[2], *Fellow, IEEE*, Dominique Dallet[3], *Member, IEEE,*

[1]Department of Measurements and Optical Electronics,
Politehnica University Timişoara, Timişoara, Romania,
E-mail: *daniel.belega@upt.ro*

[2]Department of Industrial Engineering,
University of Trento, Trento, Italy,
E-mail: *dario.petri@unitn.it*

[3]IMS Laboratory,
Bordeaux INP, University of Bordeaux, Talence, France
E-mail: *dominique.dallet@ims-bordeaux.fr*

Abstract *— This paper investigates the real-valued sine-wave amplitude and phase estimates returned by two Frequency-domain Linear Least-Squares (FLLS) algorithms. Both algorithms are based on Discrete Time Fourier Transform (DTFT) samples evaluated at the sine-wave frequency in order to maximize the immunity to wideband noise. One of the analyzed procedures, called FLLS algorithm, is affected by the contribution of the spectral image component on the estimated parameters. The other one, called enhanced-FLLS (e-FLLS) algorithm, compensates this detrimental contribution which is particularly significant when a small number of sine-wave cycles is observed. The image component interference compensation is obtained at the cost of a lightly higher computational effort and noise immunity. Closed form relationships for both the analyzed estimators and their variances are provided. Analytical expressions for the estimators which avoid matrix operations are also derived under conditions of practical interest. Finally, the accuracies of the analyzed algorithms are compared with a state-of-the-art estimator based on the classical three-parameter sine-fit algorithm, through both theoretical and simulation results.*

Index terms — Frequency-*domain analysis, least-squares approach, parameter estimation, real-valued sine-wave, windowing.*

I. INTRODUCTION

Sine-waves are often used in engineering applications because they are easy to generate and to handle mathematically. Both time-domain and frequency-domain based procedures have been proposed to estimate sine-wave parameters. Very accurate estimates of the parameters of noisy sine-waves are returned by time-domain algorithms based on the least-squares approach such as the three-parameter sine-fit (3PSF) and the four-parameter sine-fit (4PSF) algorithms [1]-[12]. The 3PSF algorithm assumes the sine-wave frequency *a-priori* known and estimates for the sine-wave amplitude, phase, and offset are obtained by means of closed form expressions [3], [10]. Conversely, the 4PSF algorithm assumes also the sine-wave frequency as an unknown parameter and it requires the implementation of an iterative procedure involving matrix operations. Therefore, the required processing effort is much higher as compared to that required by the 3PSF algorithm. When sine-waves are corrupted by a zero-mean white Gaussian noise the 3PSF and the 4PSF algorithms provide statistically efficient estimators. However, the accuracy of both estimators is negatively affected by the presence of spurious tones like harmonics and inter-harmonics and the best accuracy is achieved when coherent sampling occurs [1]-[3], [12]. To reduce the adverse effect of disturbance tones, the acquired data are firstly weighted by a suitable window function and then the adopted sine-fit algorithm is applied [4], [10]. The related procedures are called windowed sine-fit algorithms.

Many engineering applications require to accurately estimate sine-wave parameters in real-time without *a-priori* knowledge on the sine-wave frequency. In such situations the windowed 4PSF algorithm can be hardly applied due to its high processing burden. Thus, the application of the least-squares approach to frequency-domain data has been proposed in the scientific literature [13], [14]. Similarly to the time-domain approach, two different procedures have been defined: the so called Frequency-domain Linear Least-Squares (FLLS) algorithm [13] if the sine-wave frequency is known *a-priori*, and the Frequency-domain Nonlinear Least-Squares (FNLS) algorithm [14], when the sine-wave frequency must be estimated. The FLLS algorithm estimates the sine-wave amplitude and phase through close-form matrix expressions, while the FNLS algorithm requires a computationally expensive iterative procedure. However, both algorithms still require a significant computational burden. A proposal that allows a significant reduction of the processing complexity of the FLLS sine-wave parameter estimators has been recently published [15]. In that paper analytical expressions for the classical FLLS amplitude and the phase estimators have been derived in the case when a complex-valued sine-wave, three DFT samples, and the Maximum Sidelobe Decay (MSD) windows are considered [16], [17]. Also, a new FLLS algorithm which maximizes the immunity of amplitude and phase estimates to wideband noise has been proposed. It processes DTFT samples related to the normalized sine-wave frequency instead of using DFT samples as in the classical FLLS algorithm [13].

This paper aims at investigating the performance of the FLLS algorithm proposed in [15] when it is applied to real-valued sine-waves. Moreover, an algorithm which compensates the detrimental contribution of the sine-wave image component on the estimated parameters is proposed. That algorithm, called enhanced FLLS (e-FLLS) algorithm since it ensures an optimum noise immunity, while the effect of the image component doesn't need to be reduced by windowing. It is based on the rectangular window. Analytical expressions for both the frequency-domain least-squares amplitude and phase estimators and their statistical efficiencies are determined. Moreover, FLLS estimators based on the two-term MSD window and more than three DFT samples are analyzed. The accuracies of the proposed estimators and the Weighted three-Parameters Sine-Fit (W3PSF) algorithm [1]-[5] are also compared with each other.

The paper is organized as follows. In Section II both the FLLS and the e-FLLS algorithms are presented and analytical expressions for the variances of the returned estimates are obtained in the case of sine-wave corrupted by additive white Gaussian noise. Also, analytical expressions for both the FLLS algorithm based on the Hann window and the e-FLLS algorithm based on the rectangular window which avoid matrix operations are derived. In Section III the statistical efficiencies and the computational complexities of the frequency-domain least-squares algorithms and the W3PSF algorithm are compared with each other. In Section IV the accuracies of all the considered algorithms are analyzed through computer simulations when the acquired signal is affected by white Gaussian noise and harmonics. Finally, Section V concludes the paper.

II. THE FLLS AND e-FLLS ALGORITHMS

A. *The Analyzed Signal*

The analyzed real-valued discrete-time noisy sine-wave is modeled as:

$$x(m) = A\cos(2\pi fm + \phi) + r(m), \quad m = 0,1,\ldots,M-1 \tag{1}$$

where A, f, and ϕ are the sine-wave amplitude, normalized frequency, and initial phase, $r(\cdot)$ is a wideband noise, assumed to be white, Gaussian with zero mean and variance σ^2, and M is the number of acquired samples. The normalized frequency f is defined as:

$$f = \frac{f_{in}}{f_s} = \frac{\nu}{M} = \frac{l+\delta}{M}, \tag{2}$$

where f_{in} and f_s are the continuous-time sine-wave frequency and sampling rate, respectively, $\nu = l + \delta$ is the number of acquired sine-wave cycles or the normalized frequency expressed in bins, l is its integer part and δ ($-0.5 \le \delta < 0.5$) represents the inter-bin frequency location. The normalized frequency f is assumed to

satisfy the Nyquist theorem, i.e. $f \leq 0.5$. It is worth noticing that, using DFT-based algorithms, the most accurate sine-wave parameter estimates are obtained when coherent sampling occurs, i.e. $\delta = 0$. Indeed, in such a condition the detrimental contribution on the returned estimates due to the sine-wave image component is null. Unfortunately, in practice non-coherent sampling usually occurs, i.e. $\delta \neq 0$ [13].

To reduce that contribution and those of possible spurious tones such as harmonics and interharmonics, the analyzed signal $x(m)$ is multiplied by a suitable window sequence $w(m)$. The widely used cosine class windows is considered in the following [16], [18]. The generic H-term cosine window is defined as [16]-[20]:

$$w(m) = \sum_{h=0}^{H-1} (-1)^h a_h \cos\left(2\pi h \frac{m}{M}\right), \quad m = 0, 1, \ldots, M-1 \tag{3}$$

where a_h, $h = 0, 1, \ldots, H-1$, are the window coefficients.

In particular, the MSD windows exhibit the highest sidelobe decay rate, equal to $6(2H-1)$ dB/octave, among all the windows with a given number H of terms. Their coefficients are [17] $a_0 = C_{2H-2}^{H-1} / 2^{2H-2}$ and $a_h = C_{2H-2}^{H-h-1} / 2^{2H-3}, \quad h = 1, 2, \ldots, H-1,$ where $C_p^q = p!/[(p-q)!\,q!]$. In particular, the two-term MSD window (for which $a_0 = a_1 = 0.5$) is known also as the Hann window [16].

The DTFT of the windowed signal $x_w(m) = x(m) \cdot w(m)$, $m = 0,1,\ldots, M-1$, is given by [19]:

$$X_w(\lambda) \stackrel{\Delta}{=} \frac{1}{M} \sum_{m=0}^{M-1} x_w(m) e^{-j2\pi m\lambda/M} = \frac{A}{2}\left[W(\lambda-\nu)e^{j\phi} + W(\lambda+\nu)e^{-j\phi}\right] + R_w(\lambda), \quad \lambda \in [0, M) \tag{4}$$

in which $W(\cdot)$ is the DTFT of the used window $w(\cdot)$ and $R_w(\cdot)$ is the DTFT of the windowed wideband noise $r_w(m) = r(m) \cdot w(m)$. It is worth noticing that the second term in the square brackets of (4) represents the sine-wave spectral image component. Moreover, for integer values of λ, Eq. (4) returns the DFT of the signal (1).

For $M >> 1$ and $|\kappa| << M$ the DTFT of the window (3) is given by [20]:

$$W(\kappa) \cong \frac{1}{M} \sum_{m=0}^{M-1} w(m) e^{-j2\pi m\kappa/M} = \frac{\sin(\pi\kappa)}{\pi} e^{-j\pi\kappa} \sum_{h=0}^{H-1} (-1)^h a_h \frac{\kappa}{\kappa^2 - h^2}. \tag{5}$$

B. *The FLLS Algorithm*

The FLLS algorithm considers $2J + 1$ samples of the windowed signal DTFT evaluated at the known normalized frequencies $\lambda = \nu + k = l + \delta + k$, $k = -J, -J+1, \ldots, 0, \ldots, J-1, J$ [15]. Assuming that the number of acquired sine-wave cycles ν is not too small so that the contribution of the spectral image component can be neglected, from (4) we have [15]:

$$X_w(l+\delta+k) \cong BW(k) + R_w(l+\delta+k), \qquad k = -J, -J+1, \ldots, 0, \ldots J-1, J \tag{6}$$

where $B \overset{\Delta}{=} \frac{A}{2} e^{j\phi}$ is a complex number. Relationship (6) can be expressed in matrix form as [24]:

$$X_{w,J} = B\, W_J + R_{w,J}, \tag{7}$$

where

$X_{w,J} \overset{\Delta}{=} \left[X_{w(\delta-J)}\ X_{w(\delta-J+1)} \ldots X_{w(\delta+J)}\right]^T$ with $X_{w(\delta+k)} \overset{\Delta}{=} X_w(l+\delta+k)$, $W_J \overset{\Delta}{=} \left[W(-J)\, W(-J+1) \ldots W(J)\right]^T$,

and $R_{w,J} \overset{\Delta}{=} \left[R_{w(\delta-J)}\ R_{w(\delta-J+1)} \ldots R_{w(\delta+J)}\right]^T$, with $R_{w(\delta+k)} \overset{\Delta}{=} R_w(l+\delta+k)$. In the above expressions "$(\cdot)^T$" denotes the transpose operator.

Using (5) it is easy to show that for integer values of *k* we have:

$$W(k) = \begin{cases} a_0, & if \quad k = 0 \\ (-1)^k \dfrac{a_{|k|}}{2}, & if\ |k| \le H-1 \\ 0, & if\ |k| > H \end{cases} \tag{8}$$

By applying the least-squares approach to (7) the following estimator for the complex amplitude *B* based on $2J + 1$ DTFT samples is obtained [4], [13]:

$$\hat{B}_J = (W_J^* V_J^{-1} W_J)^{-1} W_J^* V_J^{-1} X_{w,J}, \tag{9}$$

where "$(\cdot)^*$" denotes the complex conjugate transpose operator, "$(\cdot)^{-1}$" denotes the inverse operator, and V_J is the noise covariance matrix of the vector $R_{w,J}$, whose elements v_{ij}, $i, j = 1, 2, \ldots, 2J + 1$ are [15]:

$$v_{ij} = \begin{cases} 1, & if\ i = j \\ (-1)^{|i-j|} \dfrac{c_{|i-j|}}{2c_0}, & if\ 0 < |i-j| \le 2H-2 \\ 0, & if\ |i-j| > 2H-2 \end{cases} \tag{10}$$

where c_h, $h = 0, 1, \ldots, H - 1$, are the coefficients of the cosine-class squared window $w^2(m)$. In particular, $c_0 = NNPG \overset{\Delta}{=} \frac{1}{M} \sum_{m=0}^{M-1} w^2(m)$, is the Noise Normalized Power Gain of the window $w(\cdot)$ [18]. It is worth noticing that the matrix V_J is equal to the identity matrix $I_{(2J+1)}$ when the rectangular window is adopted.

From the definition of *B*, the following estimates for the sine-wave amplitude and phase are obtained:

$$\hat{A}_J = 2\,|\hat{B}_J|, \ \text{and} \ \ \hat{\phi}_J = angle\left\{\hat{B}_J\right\}. \tag{11}$$

Since the sine-wave frequency ν is assumed to be known, the vector W_J can be evaluated *a-priori* and, according to the Gauss-Markov theorem, (9) represents the Best Linear Unbiased Estimator (BLUE) of the complex amplitude *B*. The variance of that estimator is given by [4]:

$$\begin{aligned} \mathrm{var}[\hat{B}_J] &= E\left[\left|\frac{\hat{A}}{2}e^{j\hat{\phi}} - \frac{A}{2}e^{j\phi}\right|^2\right] = NNPG\cdot(W_J^* V_J^{-1} W_J)^{-1}\frac{\sigma^2}{M} \\ &= NNPG\cdot(W_J^* V_J^{-1} W_J)^{-1}\,\mathrm{var}[\hat{B}]_{CR}, \end{aligned} \tag{12}$$

where $\mathrm{var}[\hat{B}]_{CR} = \sigma^2 / M$ is the Cramér-Rao Lower Bound (CRLB) for unbiased estimators of *B* [4], while E[·] and var[·] denotes the expectation and the variance operators, respectively.

Anyway, independently of the available knowledge on the vector W_J, the variance of the estimator $\hat{B}_J$ satisfies the following:

Proposition 1:

The variance of the FLLS complex-valued amplitude estimator is given by:

$$\mathrm{var}[\hat{B}_J] \cong \frac{\mathrm{var}[\hat{A}_J]}{4} + \frac{A^2\,\mathrm{var}[\hat{\phi}_J]}{4}, \tag{13}$$

where $\mathrm{var}[\hat{A}_J]$ *and* $\mathrm{var}[\hat{\phi}_J]$ *are the variances of the sine-wave amplitude and phase estimators, respectively.*

The proof of the Proposition 1 is given in the Appendix A.

The variances of the estimators $\hat{A}_J$ and $\hat{\phi}_J$ are given by [14], [15]:

$$\mathrm{var}[\hat{A}_J] \cong NNPG\cdot(W_J^* V_J^{-1} W_J)^{-1}\frac{2\sigma^2}{M} \tag{14}$$

and

$$\mathrm{var}[\hat{\phi}_J] \cong \frac{NNPG}{M\cdot SNR}\cdot(W_J^* V_J^{-1} W_J)^{-1} \tag{15}$$

when δ is known, or

$$\mathrm{var}[\hat{\phi}_J] \cong \frac{NNPG}{M\cdot SNR}\cdot(W_J^* V_J^{-1} W_J)^{-1} + \pi^2\,\mathrm{var}[\hat{\delta}], \tag{16}$$

when δ is estimated *a-priori*. In the above expressions $\mathrm{var}[\hat{\delta}]$ represents the variance of the frequency estimator $\hat{\delta}$, and $SNR \overset{\Delta}{=} A^2/(2\sigma^2)$ is the Signal-to-Noise Ratio. Moreover, when a not too small number of

sine-wave cycles is observed, the CRLBs for unbiased amplitude and phase estimators when δ is known are $\mathrm{var}[\hat{A}]_{CR} \cong 2\sigma^2 / M$ and $\mathrm{var}[\hat{\phi}]_{CR} \cong 1/(M \cdot SNR)$, respectively [4], [6]. Thus, (14) and (15) show that the statistical efficiency of the FLLS algorithm (i.e. the ratios between the CRLB and the related estimator variance) is equal to $1/(NNPG \cdot (W_J^* V_J^{-1} W_J)^{-1})$. In particular, it is inversely proportional to the window *NNPG*, which is minimum for the rectangular window [18].

Once the window $w(\cdot)$ has been selected and J has been fixed, the factor $(W_J^* V_J^{-1} W_J)^{-1}$ and the vector $W_J^* V_J^{-1}$ can be determined *a-priori* by using (8), (10), thus avoiding matrix inversion in the calculation of the estimators $\hat{A}_J$ and $\hat{\phi}_J$, and their variances. For example, if the Hann window is adopted, for J = 1, 2, and 3 we obtain, respectively:

$$\hat{B}_1 = X_{w(\delta-1)} + 3X_{w(\delta)} + X_{w(\delta+1)}, \tag{17}$$

$$\hat{B}_2 = \frac{2}{3} X_{w(\delta-2)} + 2X_{w(\delta-1)} + 4X_{w(\delta)} + 2X_{w(\delta+1)} + \frac{2}{3} X_{w(\delta+2)}, \tag{18}$$

and

$$\hat{B}_3 = \frac{1}{2} X_{w(\delta-3)} + \frac{3}{2} X_{w(\delta-2)} + 3X_{w(\delta-1)} + 5X_{w(\delta)} + 3X_{w(\delta+1)} + \frac{3}{2} X_{w(\delta+2)} + \frac{1}{2} X_{w(\delta+3)}. \tag{19}$$

Notice that the estimator $\hat{B}_1$ has been already derived in [15]. Moreover, expressions (17)-(19) hold also when considering complex-valued sine-waves embedded in white noise. In addition, since for the Hann window we have $NNPG \cdot (W_J^* V_J^{-1} W_J)^{-1} = \frac{2J+3}{2J+2}$, (14) – (16) returns:

$$\mathrm{var}[\hat{A}_J] \cong \frac{2J+3}{2J+2} \cdot \frac{2\sigma^2}{M} \cong \frac{2J+3}{2J+2} \mathrm{var}[\hat{A}]_{CR}, \tag{20}$$

and

$$\mathrm{var}[\hat{\phi}_J] \cong \frac{2J+3}{2J+2} \cdot \frac{1}{M \cdot SNR} \cong \frac{2J+3}{2J+2} \mathrm{var}[\hat{\phi}]_{CR}, \tag{21}$$

when δ is known, or

$$\mathrm{var}[\hat{\phi}_J] \cong \frac{2J+3}{2J+2} \cdot \frac{1}{M \cdot SNR} + \pi^2 \, \mathrm{var}[\hat{\delta}], \tag{22}$$

when δ is estimated *a-priori*.

C. *The enhanced FLLS Algorithm*

When the number of observed sine-wave cycles ν is small, windowing doesn't effectively reduce the contribution of the sine-wave image component on the considered DTFT samples and (9) returns low accuracy results. In that situation accurate estimates can be obtained by taking into account the contribution of the sine-wave image component on the DTFT samples, i.e.

$$X_w(l+\delta+k) \cong BW(k) + B^* W(2l+2\delta+k) + R_w(l+\delta+k), \qquad k=-J,-J+1,\ldots,0,\ldots J-1,J \tag{23}$$

where $B^* \stackrel{\Delta}{=} \frac{A}{2} e^{-j\phi}$. This is the model adopted by the enhanced FLLS (e-FLLS) algorithm.

Expressing (23) in matrix form we have:

$$X_{w,J} = B_{e,J} W_{e,J} + R_{w,J}, \tag{24}$$

in which $B_{e,J} \stackrel{\Delta}{=} [B \;\; B_J^*]^T$, and $W_{e,J} \stackrel{\Delta}{=} \begin{bmatrix} W(-J) & W(-J+1) & \cdots & W(J) \\ W(2l+2\delta-J) & W(2l+2\delta-J+1) & \cdots & W(2l+2\delta+J) \end{bmatrix}^T$,

where the vectors $X_{w,J}$ and $R_{w,J}$ are defined as in (7).

By applying the least-squares approach to (24) the following estimator for $B_{e,J}$ is obtained [4]:

$$\hat{B}_{e,J} = (W_{e,J}^* V_J^{-1} W_{e,J})^{-1} W_{e,J}^* V_J^{-1} X_{w,J}, \tag{25}$$

where the matrix V_J is defined as in (7).

From (24), the sine-wave amplitude and phase estimators are then obtained as:

$$\hat{A}_{e,J} = 2\,|\,\hat{B}_{e,J\,1}\,| \text{ and } \hat{\phi}_{e,J} = angle\{\hat{B}_{e,J\,1}\}. \tag{26}$$

In (26) the first element $\hat{B}_{e,J_1}$ of the complex vector $\hat{B}_{e,J}$ is used since it is related to the sine-wave positive frequency component (i.e. to the first term in (23)) whose contribution dominates the DTFT values at the considered frequencies.

When the inter-bin frequency location δ is known, the matrix $W_{e,J}$ can be evaluated and, according to the Gauss-Markov theorem, $\hat{B}_{e,J}$ represents the BLUE for the complex-valued vector amplitude B_e = [B, B*]. Its variance is given by [4]:

$$\text{var}[\hat{B}_{e,J}] = NNPG \cdot (W_{e,J}^* V_J^{-1} W_{e,J})^{-1} \frac{\sigma^2}{M}, \tag{27}$$

In particular, for $\hat{B}_{e,J_1}$ we have:

$$\begin{aligned}\mathrm{var}[\hat{B}_{e,J_1}] &= NNPG \cdot \left[(W_{e,J}^{*} V_J^{-1} W_{e,J})^{-1}\right]_{11} \frac{\sigma^2}{M} \\ &= NNPG \cdot \left[(W_{e,J}^{*} V_J^{-1} W_{e,J})^{-1}\right]_{11} \mathrm{var}[\hat{B}]_{CR}.\end{aligned} \tag{28}$$

Unlike the FLLS algorithm, explicit expressions for the e-FLLS estimators can be hardly obtained since the matrix $W_{e,J}$ contains also the elements $W(2l + 2\delta + k)$, $k = -J, -J + 1, \ldots, 0, \ldots, J - 1, J$. However, when few sine-wave cycles are acquired it makes sense to consider the rectangular window since the effect of the image component is taken into account in the model (23) and a different windowing would result in lower immunity to wideband noise. In that case, the following Proposition holds:

Proposition 2:

The expression for the e-FLLS complex-valued amplitude estimator based on the rectangular window is given by:

$$\hat{B}_{e,J_1} = X_{w(\delta)} - \sum_{\substack{k=-J \\ k\neq 0}}^{J} \frac{W^{*}(2l + 2\delta + k) \cdot W(2l + 2\delta)}{\Delta_J} \cdot X_{w(\delta+k)}, \tag{29}$$

where $\Delta_J \overset{\Delta}{=} \sum_{\substack{k=-J \\ k\neq 0}}^{J} \left|W(2l + 2\delta + k)\right|^2$.

The proof of the Proposition 2 is given in the Appendix B.

In addition, the following Propositions hold about the variances of the estimates returned by the e-FLLS algorithm based on the rectangular window when the number of observed cycles ν is high enough.

Proposition 3:

If the sine-wave frequency is known, the variance of the e-FLLS complex-valued amplitude estimator based on the rectangular window and a high number of observed sine-wave cycles is given by:

$$\mathrm{var}[\hat{B}_{e,J_1}] \cong \frac{2J+1}{2J} \cdot \frac{\sigma^2}{M} \cong \frac{2J+1}{2J} \cdot \mathrm{var}[\hat{B}]_{CR}. \tag{30}$$

Proposition 4:

The variances of the e-FLLS amplitude and phase estimators based on the rectangular window and a high number of observed sine-wave cycles are given by:

$$\mathrm{var}[\hat{A}_{e,J}] \cong \frac{2J+1}{2J} \cdot \frac{2\sigma^2}{M} \cong \frac{2J+1}{2J} \mathrm{var}[\hat{A}]_{CR}, \tag{31}$$

and

$$\mathrm{var}[\hat{\phi}_{e,J}] \cong \frac{2J+1}{2J} \cdot \frac{1}{M \cdot SNR} \cong \frac{2J+1}{2J} \mathrm{var}[\hat{\phi}]_{CR}, \tag{32}$$

when δ is known, or

$$\mathrm{var}[\hat{\phi}_J] \cong \frac{2J+1}{2J} \cdot \frac{1}{M \cdot SNR} + \pi^2 \mathrm{var}[\hat{\delta}], \tag{33}$$

when δ is estimated *a-priori*.

The proofs of the Propositions 3 and 4 are given in the Appendices C and D, respectively.
The application of the e-FLLS estimators is advantageous when the contribution of the image component to the estimates returned by the FLLS algorithm is higher than the effect of wideband noise.

D. *Statistical efficiency of the frequency-domain least-squares algorithms*

By comparing expressions (31) – (33) and (20) – (22) it follows that, for a given value of *J*, when enough sine-wave cycles are observed, the variances of the amplitude and phase estimators returned by the e-FLLS algorithm based on the rectangular window and (2*J* + 3) DTFT samples or the FLLS algorithm based on the Hann window and (2*J* + 1) DTFT samples coincide.

Table I shows the theoretical statistical efficiencies (i.e. the ratios between the CRLB and the related estimator variance) of the amplitude and the phase estimators provided by the FLLS algorithm based on the Hann window and the e-FLLS algorithm based on the rectangular window assuming that the sine-wave frequency is known and that enough sine-wave cycles are observed. Different values for the number 2*J* + 1 of processed DTFT samples are considered.

As expected, the FLLS estimator immunity to wideband noise decreases as the window order increases. Anyway, values quite close to the CRLB can be achieved by increasing the number of DTFT samples, but at the cost of a higher computational effort. Observe also that, to increase the estimation accuracy, the effect of possible spurious tones on the 2*J* + 1 DTFT processed samples must be negligible. Thus, the highest value of *J* that can be considered could be limited by the number of observed sine-wave cycles.

Table I. Statistical efficiencies of the amplitude and the phase estimators provided by the FLLS algorithm based on the Hann window and e-FLLS algorithm based on the rectangular window. Sine-wave frequency known *a-priori* and a high number of observed sine-wave cycles.

Number of DTFT processed samples ($2J+1$)	3	5	7	11	21
FLLS based on Hann window	0.800	0.857	0.889	0.923	0.956
e-FLLS based on rectangular window	0.667	0.800	0.857	0.909	0.952

III. FREQUENCY-DOMAIN LEAST-SQUARES AND W3PSF ALGORITHMS: COMPARISON OF THE STATISTICAL EFFICIENCY AND THE COMPUTATIONAL COMPLEXITY

The W3PSF algorithm is the classical three-parameter sine-fit algorithm [1]-[5] applied to windowed data in order to reduce the effect of spurious tones that may affect the acquired sine-wave samples [4]. That algorithm has been chosen as a benchmark since it requires a low computational effort although providing optimum noise immunity when the rectangular window is used. According to the best of the authors' knowledge, its main drawback is due to the low immunity to spurious tones like harmonics and inter-harmonics, especially when the rectangular window is used.

Assuming that the number of observed sine-wave cycles ν is high enough that the interference from the sine-wave image component can be neglected, the variances of the estimators $\widetilde{A}$ and $\widetilde{\phi}$ returned by the W3PSF algorithm are given by [10]:

$$\mathrm{var}[\widetilde{A}] \cong ENBW_0 \frac{2\sigma^2}{M} \cong ENBW_0 \, \mathrm{var}[\hat{A}]_{CR}, \tag{34}$$

and

$$\mathrm{var}[\widetilde{\phi}] \cong ENBW_0 \cdot \frac{1}{M \cdot SNR} \cong ENBW_0 \, \mathrm{var}[\hat{\phi}]_{CR}, \tag{35}$$

when δ is known, or

$$\mathrm{var}[\widetilde{\phi}] \cong ENBW_0 \frac{1}{M \cdot SNR} + \pi^2 \, \mathrm{var}[\hat{\delta}], \tag{36}$$

when δ is estimated *a-priori*. In (34)-(36), $ENBW_0 \overset{\Delta}{=} M \sum_{m=0}^{M-1} w_0^2(m) \Big/ \left(\sum_{m=0}^{M-1} w_0(m) \right)^2$ is the Equivalent Noise BandWidth of the squared window $w_0(m) = w^2(m)$. Since $ENBW_0 = 1$ for the rectangular window, the W3PSF algorithm provides almost efficient amplitude and phase estimators when δ is known or it is

estimated using an efficient estimator [4]. Conversely, statistical efficiency does not longer hold if the Hann window (whose $ENBW_0$ is equal to 35/18) is used.

When the inter-bin frequency location δ is known, using (14) and (34) or (15) and (35), it results that the ratios between the variances of the amplitude or the phase estimators returned by the FLLS algorithm and the W3PSF algorithm are given by:

$$\frac{\mathrm{var}[\hat{A}_J]}{\mathrm{var}[\tilde{A}]} \cong \frac{\mathrm{var}[\hat{\phi}_J]}{\mathrm{var}[\tilde{\phi}]} \cong \frac{M^2 \cdot NNPG \cdot (W_J^* V_J^{-1} W_J)^{-1}}{ENBW_0}. \tag{37}$$

When the Hann window is adopted, from (20), (21), (34), and (35), (37) we have:

$$\frac{\mathrm{var}[\hat{A}_J]}{\mathrm{var}[\tilde{A}]} \cong \frac{\mathrm{var}[\hat{\phi}_J]}{\mathrm{var}[\tilde{\phi}]} \cong \frac{2J+3}{2J+2} \cdot \frac{1}{ENBW_0}. \tag{38}$$

That expression shows that the FLLS algorithm based on the Hann window exhibits a smaller immunity to wideband noise than the W3PSF algorithm based on the rectangular window (for which $ENBW_0 = 1$), but it outperforms the W3PSF algorithm based on the Hann window (in that case (38) returns 18/35 +9/(35(J+1))).

Moreover, using (31) and (34) or (32) and (35) it results that the ratios between the variances of the amplitude and the phase estimators returned by the e-FLLS algorithm based on the rectangular window and the W3PSF algorithm are given by:

$$\frac{\mathrm{var}[\hat{A}_J]}{\mathrm{var}[\tilde{A}]} \cong \frac{\mathrm{var}[\hat{\phi}_J]}{\mathrm{var}[\tilde{\phi}]} \cong \frac{2J+1}{2J} \cdot \frac{1}{ENBW_0}. \tag{39}$$

That expression shows that the e-FLLS algorithm based on the rectangular window exhibits a smaller immunity to wideband noise than the W3PSF algorithm based on the rectangular window (the ratio (39) becomes 1+1/(2J)), but it outperforms the W3PSF algorithm based on the Hann window (in that case (39) becomes 18/35+9/(35J)).

As for the computational complexity, Table II shows the number of elementary operations required by the FLLS algorithm based on the Hann window, the e-FLLS algorithm based on the rectangular window, the W3PSF algorithm based on the rectangular or a non-rectangular window. The sine-wave frequency is assumed to be known *a-priori* and $2J + 1$ DTFT samples are used in the frequency-domain least-squares algorithms. In the e-FLLS algorithm, the DTFT of the rectangular window is computed using (5) and noticing that the terms $W^*(2l + 2\delta + k) \cdot W(2l + 2\delta)$ in (29) are real-valued. For the W3PSF algorithm, the analytical expressions for the sine-wave amplitude and phase estimators reported in [3] have been considered.

Table II. Computational complexity of the complex amplitude estimators returned by the FLLS algorithm based on the Hann window, the e-FLLS algorithm based on the rectangular window, and the W3PSF algorithm based on the rectangular or a non-rectangular window. Sine-wave frequency known *a-priori*. $2J + 1$ DTFT samples processed by the frequency-domain least-squares algorithms.

Algorithm	***Elementary operations***			
	real additions	*real multiplications*	*trigonometric functions*	*real divisions*
FLLS - Hann window	$2M(2J + 1) - 2$	$2M(2J+1.5)+4J+2$	$2M(2J + 1)$	-
e-FLLS - rect. window	$2M(2J + 1) - 4$	$2M(2J + 1)+ 8J$	$2M(2J + 1)+2J + 1$	$2J + 3$
W3PSF - rect. window	$2M + 3$	$2M + 12$	$2M + 1$	4
W3PSF - non-rect. window	$4M$	$8M + 9$	$2M$	2

Since in practice $M >> J$, Table II shows that both considered frequency-domain least squares estimators require almost $2M(2J + 1)$ real additions, multiplications, and trigonometric functions. The e-FLLS estimator $\hat{B}_{e,J_1}$ requires also $2J + 3$ real divisions. Also, the e-FLLS and FLLS algorithms require a higher processing effort than the W3PSF algorithm based on the rectangular window, which is the least computationally demanding algorithm, and the W3PSF algorithm based on a non-rectangular window.

IV. COMPUTER SIMULATIONS

In this Section, the accuracies of the FLLS, the e-FLLS, and the W3PSF algorithms are compared with each other. In the performed computer simulations estimation accuracy is quantified by the Root of the Mean Square Error (RMSE) and the following conditions and parameters are considered:

- sine-wave with amplitude $A = 1$, affected by either additive white Gaussian noise only or both noise and harmonics; the *SNR* is 40 dB and the Total Harmonic Distortion (*THD*) ratio is equal to 8%; only the 2nd and the 3rd harmonics are considered, with amplitudes in the ratio 2:1, respectively; indeed their effect on the estimated parameters is much stronger than higher order harmonics due to their closeness to the fundamental frequency;
- both few and many acquired sine-wave cycles are considered, that is ν varies in the range [1.51, 6) or [15.51, 20) cycles, respectively, with a step of 0.05 cycles;
- both the rectangular and the Hann windows are used in the e-FLLS algorithm, while only the Hann window is adopted in the FLLS algorithm due to the relevant contribution of the image component on the estimated parameters when the rectangular window is used;
- both the rectangular and the Hann windows are considered in the W3PSF algorithm;

- both FLLS and e-FLLS algorithms based on 3 or 5 DTFT samples (i.e. $J = 1$ or $J = 2$) are considered; the complex-valued amplitude FLLS estimator is obtained by applying (17) and (18), respectively; the e-FLLS estimator based on the rectangular window is returned by (29), while that based on the Hann window is obtained using (25);
- both known and unknown sine-wave frequency are considered; when the sine-wave frequency is unknown, it is estimated *a-priori* by two iterations of the Aboutanios and Mulgrew (AM) algorithm [21] based on the Hann window and the DTFT sample modules [22], [23]; that algorithm has been chosen since it provides an unbiased frequency estimator and the related variance is equal to the minimum value returned by the Interpolated DFT (IpDFT) frequency estimator which, for the Hann window, is given by [23]:

$$\mathrm{var}[\hat{\delta}] \cong \frac{81\pi^2}{1024} \cdot \frac{1}{M \cdot SNR}. \tag{40}$$

Monte Carlo simulations based on 1000 runs of $M = 512$ samples of a sine-wave with phase varying at random are considered.

When the sine-wave frequency is known, simulations showed that the variances of the FLLS or the e-FLLS amplitude and phase estimators exhibit the same behavior, thus confirming the theoretical results derived in Subsections II.B and II.C. Conversely, when the sine-wave frequency is unknown, the variances of all the considered phase estimators are dominated by the frequency estimation errors, i.e. the term $\pi^2 \,\mathrm{var}[\hat{\delta}]$ in expressions (16), (22), and (33) prevails on the other term. Thus, only the RMSEs of the amplitude estimators are analyzed in the following.

Moreover, simulations showed that in this case the e-FLLS algorithm based on the rectangular window provides more accurate results than the FLLS algorithm based on the Hann window when ν is smaller than about $0.18 \cdot SNR - 0.22$ or $0.19 \cdot SNR + 0.92$ if $J = 1$ or $J = 2$, respectively, where *SNR* is given in dB. Thus, for $SNR = 40$ dB the e-FLLS algorithm provides more accurate estimates than the FLLS algorithm when ν is less than 7 or 8.5 cycles when $J = 1$ and $J = 2$, respectively.

Many other simulations were performed considering different conditions and MSD windows with a higher number of terms. A good agreement between simulation and theoretical results was always achieved.

A. Accuracy comparison between the FLLS and the e-FLLS algorithms

Fig. 1 shows the RMSEs of the amplitude estimators returned by the e-FLLS and the FLLS algorithms in the case of noisy sine-waves when few cycles are observed. The sine-wave frequency is assumed either known or unknown. Moreover, the theoretical variances related to the FLLS algorithm

based on the Hann window and the e-FLLS algorithm based on the rectangular window returned by (20) and (31), respectively, and the square root of the related CRLB are shown.

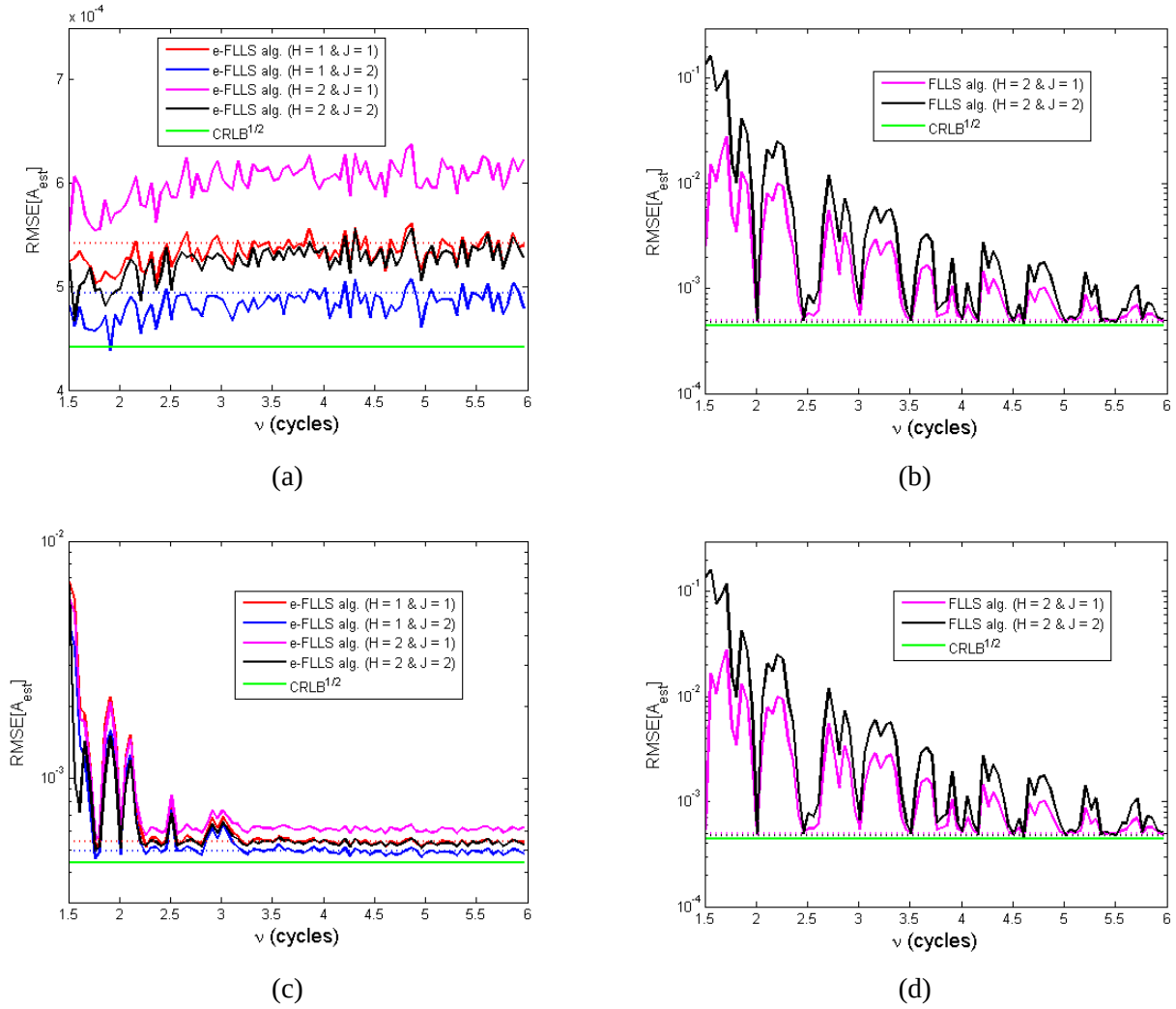

Fig. 1. Noisy sine-waves: *RMSE*s of the amplitude estimators provided by the e-FLLS algorithm based on the rectangular or the Hann windows, $J = 1$ or 2 (a) and (c), and the FLLS algorithm based on the Hann window, $J = 1$ or 2 (b) and (d) versus ν in the range [1.51, 6) cycles. The sine-wave frequency is assumed to be known (a) and (b), or unknown and estimated by the AM algorithm based on the Hann window (c) and (d). The theoretical variance (20) for the FLLS algorithm based on the Hann window or the theoretical variance (31) for the e-FLLS algorithm based on the rectangular window are shown using dotted lines. The square root of the CRLB is also reported. $SNR = 40$ dB, 1000 simulation runs of $M = 512$ samples each.

When the sine-wave frequency is known, Fig. 1(a) and (b) show that the e-FLLS algorithm largely outperforms the FLLS algorithm since the values returned by the latter are heavily affected by the contribution of the spectral image component. Moreover, the RMSEs of the e-FLLS algorithm are almost independent of the number of acquired sine-wave cycles ν, the accuracy increases as the number of

processed DTFT samples, i.e. J, increases. The e-FLLS algorithms provide an effective compensation of the contribution of the spectral image component, which is negligible as compared with the effect of noise. Therefore, for a given value of J, the e-FLLS estimator based on the rectangular window outperforms the one based on the Hann window. The best accuracy is provided by the e-FLLS algorithm based on the rectangular window and $J = 2$. Also, it can e observed that the e-FLLS algorithm based on the Hann window and $J = 2$ has almost the same accuracy as the e-FLLS algorithm based on the rectangular window and $J = 1$. In addition, Fig. 1(b) shows that the RMSEs related to the FLLS algorithm based on the Hann window are much higher than the theoretical variances due to noise. This occurs because of the detrimental contribution of the sine-wave image component.

When the sine-wave frequency is unknown and estimated by the AM algorithm, Fig. 1(c) shows that the amplitude estimates returned by the e-FLLS algorithm are quite inaccurate when very few sine-wave cycles are acquired. This is due to the effect of the image component on the AM frequency estimator. Conversely, when ν is greater than about 3 cycles the AM algorithm returns accurate frequency estimates and the e-FLLS amplitude estimators exhibit the same accuracy as in Fig. 1(a). As for the FLLS amplitude estimators, the RMSE values are always heavily affected by the contribution of the image component so that the curves reported in Fig. 1(b) and (d) are close with each other.

Concluding, the e-FLLS algorithm largely outperforms the FLLS algorithm in all the situations considered above since it models the contribution of the sine-wave image component.

Fig. 1 also shows that the RMSEs provided by the FLLS and the e-FLLS algorithms are always higher than the square root of the related CRLB, due to windowing, the contribution from the image component or the small number of processed DTFT samples. In addition, simulations confirm the theoretical expressions derived in Subsection II.B for the estimator statistical efficiencies.

Fig. 2 is related to the same simulation conditions as in Fig. 1, but a high number of sine-wave cycles ν is observed. In this case the sine-wave frequency is estimated very accurately by the AM algorithm so that the related amplitude estimate RMSEs almost coincide with those obtained for known frequency. Thus, they are not reported in Fig. 2.

As specified above, the e-FLLS estimators are mainly affected by wideband noise since they compensate the contribution of the spectral image component. As a consequence, for a given value of J, the e-FLLS algorithm based on the rectangular window outperforms that based on the Hann window - as shown in Fig. 2(a) - since the former exhibits a higher noise immunity.

Unlike Fig. 1, there is a very good agreement between simulation and theoretical results for all the considered values of ν since the contribution of the spectral image component on the returned amplitude estimates is negligible as compared to the effect of wideband noise.

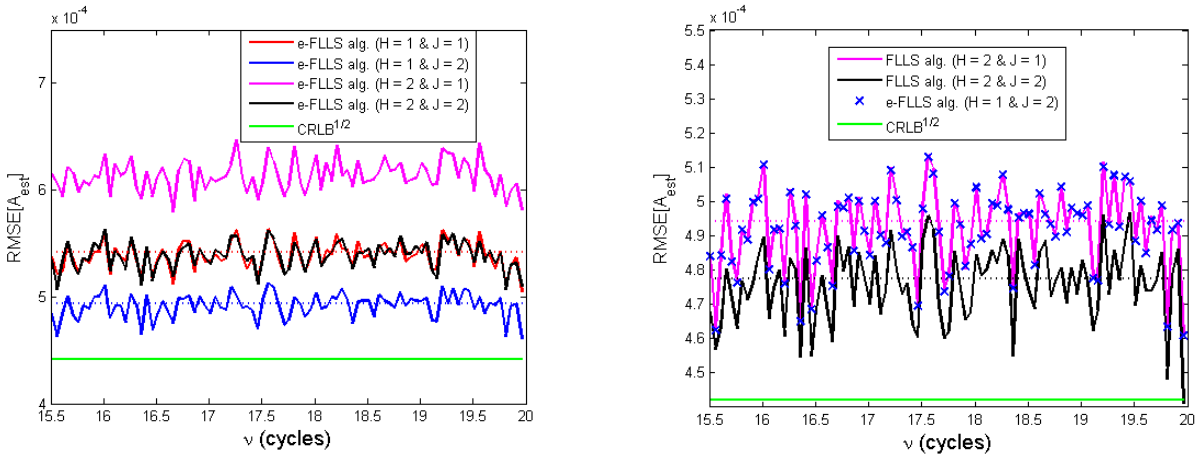

(a) (b)

Fig. 2. Noisy sine-waves: *RMSE*s of the amplitude estimators provided by the e-FLLS algorithm based on the rectangular or the Hann windows, $J = 1$ or 2 (a), the FLLS algorithm based on the Hann window with $J = 1$ or 2 and the e-FLLS algorithm based on the rectangular window with $J = 2$ (b) versus ν in the range [15.51, 20) cycles. The sine-wave frequency is assumed to be known. The theoretical variance (20) for the FLLS algorithm based on the Hann window or the theoretical variance (31) for the e-FLLS algorithm based on the rectangular window are shown using dotted lines. The square root of the CRLB is also reported. *SNR* = 40 dB, 1000 simulation runs of $M = 512$ samples each.

Results similar to those reported in Figs. 1 and 2 have been obtained for different values of *SNR* higher than 20 dB. The main difference with respect to the above figures is that the value of the number of acquired sine-wave cycles ν above which the contribution of wideband noise dominates so that the RMSEs returned by simulations almost coincide with the theoretical variances, increases as *SNR* increases.

Fig. 3 shows the simulated RMSEs returned by the considered algorithms and the theoretical variances (20) and (31) related to the FLLS algorithm based on the Hann window and the e-FLLS algorithm based on the rectangular window, respectively, in the case of noisy and harmonically distorted signals when the sine-wave frequency is known and few sine-wave cycles are observed. The square roots of the unbiased CRLBs related to the fundamental component are also reported. Behaviors very similar to those reported in Fig. 3 were observed when the sine-wave frequency is unknown. Indeed, the detrimental contribution of harmonics dominates the estimation error when few sine-wave cycles are observed, while when the number of cycles ν is high enough the effect of wideband noise or the contribution of the image component prevail for the e-FLLS estimator or the FLLS algorithm, respectively. Consequently, the related results are not reported in the paper.

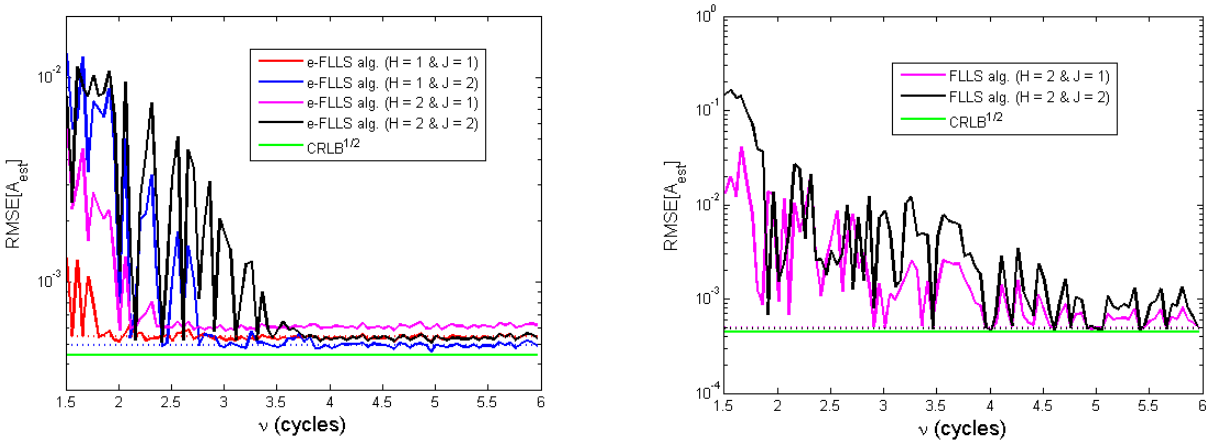

(a) (b)

Fig. 3. Noisy and harmonically distorted sine-waves: *RMSE*s of the amplitude estimators provided by the e-FLLS algorithm based on the rectangular or the Hann windows, $J = 1$ or 2 (a), and the FLLS algorithm based on the Hann window, $J = 1$ or 2 (b) versus ν in the range [1.51, 6) cycles. The sine-wave frequency is assumed to be known. The theoretical variance (20) for the FLLS algorithm based on the Hann window or the theoretical variance (31) for the e-FLLS algorithm based on the rectangular window are shown using dotted lines. The square root of the CRLB related is also reported. *SNR* = 40 dB, *THD* = 8% and 1000 simulation runs of $M = 512$ samples each.

Fig. 3 shows that the e-FLLS algorithm outperforms the FLLS algorithm. For very small values of ν, the e-FLLS algorithm provides better results when $J = 1$ since the considered DTFT samples are less affected by harmonics than the additional samples processed when using $J = 2$. For the considered *THD* and *SNR* values, the best accuracy is obtained by the e-FLLS algorithm based on the rectangular window and $J = 1$ when $\nu < 2.75$ cycles or $J = 2$ for the remaining values of ν. When ν is greater than about 3.5 cycles, the e-FLLS algorithm exhibit almost the same accuracy as in the case of noisy signals, since the effect of harmonics becomes negligible.

B. Accuracy comparison between the frequency-domain least-squares and the W3PSF algorithms

The accuracies of the FLLS, the e-FLLS, and the W3PSF algorithms are compared with each other by considering the same signals used in the previous subsection. Only the results related to the FLLS algorithms that provides the better accuracy are reported in the following, that is the e-FLLS algorithm based on the rectangular window when few sine-wave cycles are observed, or the FLLS algorithm based on the Hann window when the number of observed cycles is high enough that the contribution of the image component can be neglected.

Fig. 4 shows the RMSEs and the theoretical variances of the amplitude estimators returned by the e-FLLS algorithm based on the rectangular window and $J = 1$ or $J = 2$, and the W3PSF algorithm based on the

rectangular or the Hann windows when few sine-wave cycles are observed. The considered noisy sine-waves are the same as in Fig. 1.

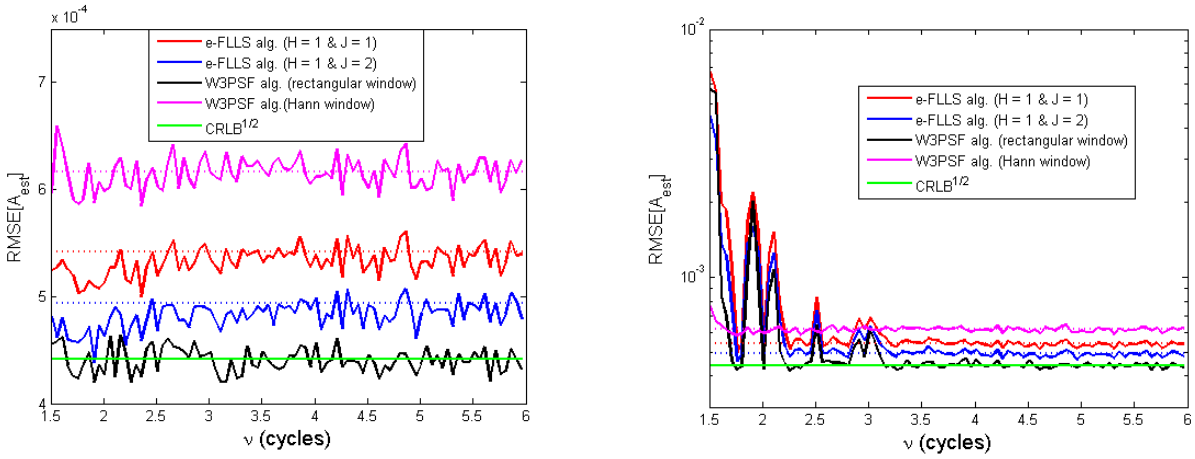

(a) (b)

Fig. 4. Noisy sine-waves: *RMSEs* and theoretical variances of the amplitude estimators provided by the e-FLLS algorithm based on the rectangular window and the W3PSF algorithm based on the rectangular or the Hann windows versus ν in the range [1.51, 6) cycles. The sine-wave frequency is assumed to be known (a) or unknown and estimated by the AM algorithm based on the Hann window (b). The theoretical variance (31) for the e-FLLS algorithm or the theoretical variance (34) for the W3PSF algorithm are shown using dotted lines. The square root of the CRLB is also reported. *SNR* = 40 dB, 1000 simulation runs of M = 512 samples each are considered.

When the sine-wave frequency is known the W3PSF algorithm based on the rectangular window outperforms the others since it returns a statistically efficient amplitude estimator [4]. It is worth noticing that the results returned by simulations seem to contradict a well-established theory since the obtained RMSE values are sometimes below the related CRLB. However, this is a statistical effect due to the finite number of processed data, as clearly shown by simulations performed using a higher number of ~~runs acquired samples.~~ runs

In Fig. 4, the poorest accuracy is provided by the W3PSF algorithm based on the Hann window. When the sine-wave frequency is unknown and estimated by the AM algorithm, all the considered amplitude estimators provide poor accuracy when $\nu < 2.25$ cycles since the AM algorithm returns poor frequency estimates. Conversely, RMSE values very close to those related to known sine-wave frequency are obtained when at least 3 sine-wave cycles are observed. Indeed in this situation the AM algorithm returns very accurate frequency estimates.

Fig. 5 shows the simulated RMSEs and the theoretical variances returned by the FLLS amplitude estimator based on the Hann window and J = 1 or J = 2, and the W3PSF algorithm based on the rectangular or the Hann windows when at least 15.5 sine-wave cycles are observed. The same noisy sine-waves as in Fig. 2 are considered and the sine-wave frequency is assumed to be known.

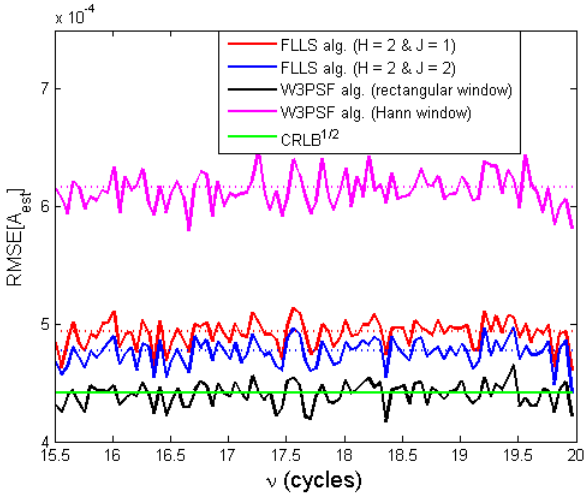

Fig. 5. Noisy sine-waves: *RMSEs* and theoretical variances of the amplitude estimators provided by the FLLS algorithm based on the Hann window and the W3PSF algorithm based on the rectangular or the Hann windows versus ν the range [15.51, 20) cycles. The sine-wave frequency is assumed to be known. The theoretical variance (20) for the FLLS algorithm or the theoretical variance (34) for the W3PSF algorithm are shown using dotted lines. The square root of the CRLB is also reported. *SNR* = 40 dB, 1000 simulation runs of M = 512 samples each.

Again the W3PSF algorithm based on the rectangular window outperforms the others since it provides statistically efficient amplitude estimators [4]. However, the accuracies of the FLLS amplitude estimators are quite close to the optimal one. The same RMSE values as in Fig. 5 are obtained when the sine-wave frequency is unknown since in the considered conditions the AM algorithm returns very accurate frequency estimates.

Fig. 6 shows the RMSEs of the amplitude estimators returned by the e-FLLS algorithm based on the rectangular window and J = 1 or J = 2 and the W3PSF algorithm based on the rectangular or the Hann windows when the same noisy and harmonically distorted sine-waves employed in Fig. 3 are considered. When the sine-wave frequency is known, Fig. 6(a) shows that the e-FLLS algorithm outperforms the W3PSF algorithm. The e-FLLS algorithm exhibits the best accuracy when $\nu < 3$ cycles and J = 1, while the two considered e-FLLS algorithms provide very close accuracies for higher values of ν. The W3PSF algorithm based on the Hann window or the W3PSF algorithm based on the rectangular window provide the worst accuracy when ν is lower or higher than 2 cycles, respectively. When the sine-wave frequency is unknown, Fig. 6(b) shows that the e-FLLS algorithm exhibits high RMSE values for $\nu < 2$ cycles since the AM algorithm returns inaccurate frequency estimates due to the contribution of the image component and harmonics. Conversely, when at least 2 sine-wave cycles are observed, the estimated frequency is accurate and the RMSE values returned by all the considered algorithms are very close to those reported in Fig. 6(a) for known sine-wave frequency.

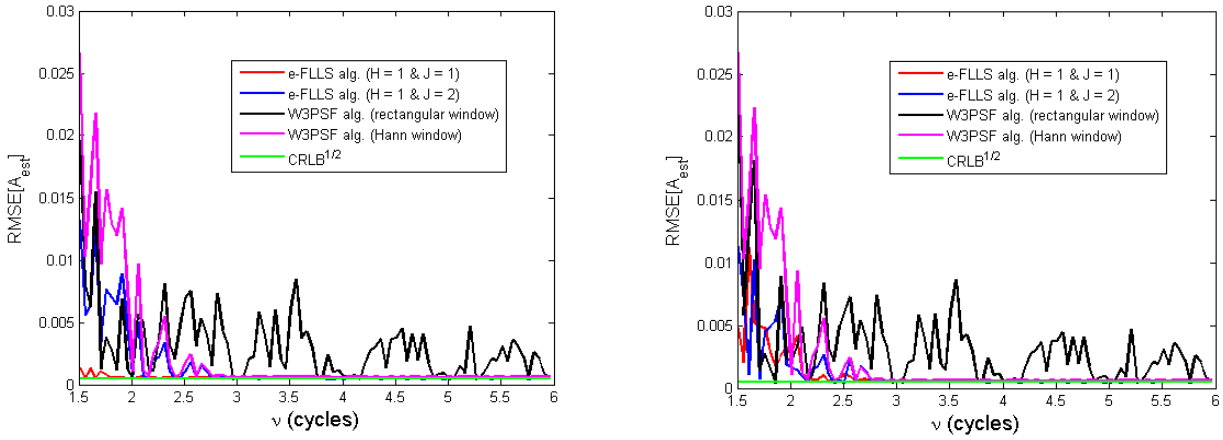

(a) (b)

Fig. 6. Noisy and harmonically distorted sine-waves: *RMSE*s of the amplitude estimators provided by the e-FLLS algorithm based on the rectangular window and the W3PSF algorithm based on the rectangular or the Hann windows versus ν in the range [1.51, 6) cycles. The sine-wave frequency is assumed to be known (a) or unknown and estimated by the AM algorithm based on the Hann window (b). The square root of the CRLB is reported. *SNR* = 40 dB, *THD* = 8% and 1000 simulation runs of M = 512 samples each.

The processing times required by the all the considered algorithms have been compared each other also through simulations performed in MATLAB 7.1 environment. A portable computer with a 2.6 GHz processor, 4 GB RAM memory, equipped with a Microsoft Windows 8.1 has been used, the DTFT samples have been computed using the formula (4) and the sine-wave frequency is assumed *a-priori* known. In such conditions the average processing times required to process 10,000 runs by the FLLS algorithm based on the Hann window and the e-FLLS algorithm based on the rectangular window are about 0.19 ms and 0.23 ms for J = 1 and 0.28 ms and 0.29 ms for J = 2, respectively, while those required by the W3PSF algorithm based on the rectangular and Hann windows are 0.06 ms and 0.19 ms, respectively.

Thus, coherently with the computationally complexity analysis performed in Section III, the smallest processing time is achieved by the W3PSF algorithm based on the rectangular window, while the FLLS and e-FLLS algorithms exhibit a higher processing times than the W3PSF algorithm based on the Hann window when J = 2. Moreover, when J = 1, the FLLS algorithm, the e-FLLS algorithm, and the W3PSF algorithm based on the Hann window require close processing times.

V. CONCLUSIONS

In this paper the accuracy of the real-valued sine-wave amplitude and the phase estimates returned by frequency-domain least-squares algorithms has been investigated. Moreover, to compensate the detrimental

contribution of the image component on the obtained estimates the e-FLLS algorithm has been proposed. Analytical expressions for the amplitude and the phase estimators returned by the FLLS algorithm based on the Hann window and the e-FLLS algorithm based on the rectangular window which avoid matrix operations have been derived, thus improving algorithm real-time capabilities. Analytical expressions have been provided also for the estimator variances due to wideband noise. For a fixed value of J, it has been shown that the e-FLLS estimator based on the rectangular window and $(2J + 3)$ DTFT samples, and the FLLS estimator based on the Hann window and $(2J + 1)$ DTFT samples exhibit the same accuracy when the number of acquired sine-wave cycles is high enough. Also, computer simulations showed that the e-FLLS algorithm outperforms the FLLS algorithm when a small number of sine-wave cycles is observed, while the latter algorithm prevails for long observation intervals. In addition, the e-FLLS algorithm based on the rectangular window requires a bit smaller processing effort than the FLLS algorithm based on the Hann window. As compared with the W3PSF algorithm, the analyzed frequency-domain least-squares algorithms require processing efforts close to that of the W3PSF algorithm based on a non-rectangular window. Also, they exhibit a higher immunity to wideband noise when the Hann window is used in the W3PSF algorithm or a slightly smaller immunity when the rectangular window is adopted in the W3PSF algorithm. Finally, the e-FLLS algorithm is more robust to harmonics than the W3PSF algorithm.

APPENDIX A

Proof of the Proposition 1

The estimated complex-valued amplitude can be written as:

$$\hat{B}_J = \frac{\hat{A}_J}{2} e^{j\hat{\phi}_J} = \frac{A + \Delta A_J}{2} e^{j(\phi + \Delta\phi_J)}, \tag{A.1}$$

where $\Delta A_J \overset{\Delta}{=} \hat{A}_J - A$ and $\Delta\phi_J \overset{\Delta}{=} \hat{\phi}_J - \phi$ are the amplitude and the phase estimation errors, respectively.

Expanding (A.1) in Taylor's series around the true values A_J and ϕ_J and considering only the first order terms, we have:

$$\hat{B}_J = \frac{\hat{A}_J}{2} e^{j\hat{\phi}_J} \cong \frac{A}{2} e^{j\phi} + \frac{\Delta A_J}{2} e^{j\phi_J} + j\frac{A}{2} e^{j\phi} \Delta\phi_J . \tag{A.2}$$

From (A.2) it follows that:

$$\mathrm{var}[\hat{B}_J] = E\left[\left|\frac{\hat{A}}{2} e^{j\hat{\phi}} - \frac{A}{2} e^{j\phi}\right|^2\right] \cong \frac{1}{4} E\left[\Delta^2 A_J + A^2 \Delta^2 \phi_J\right] \tag{A.3}$$

Finally, expression (13) easily follows from (A.3).

APPENDIX B

Proof of the Proposition 2

Using (8), when a rectangular window is considered we have:

$$W_{e,J} \overset{\Delta}{=} \begin{bmatrix} 0 & 0 & \dots & 0 & 1 & 0 & \dots & 0 \\ W_{i(-J)} & W_{i(-J+1)} & \dots & W_{i(-1)} & W_{i(0)} & W_{i(1)} & \dots & W_{i(J)} \end{bmatrix}^T, \tag{B.1}$$

where $W_{i(k)} \overset{\Delta}{=} W(2l + 2\delta + k)$ determines the contribution related to the sine-wave image component.

From (B.1) we obtain:

$$(W_{e,J}^* W_{e,J})^{-1} = \frac{1}{\Delta_J} \begin{bmatrix} \sum_{k=-J}^{J} \left| W_{i(k)} \right|^2 & -W_{i(0)} \\ -W_{i(0)}^* & 1 \end{bmatrix}, \tag{B.2}$$

where $\Delta_J \overset{\Delta}{=} \sum_{\substack{k=-J \\ k \neq 0}}^{J} \left| W_{i(k)} \right|^2$,

and

$$(W_{e,J}^* W_{e,J})^{-1} W_{e,J} = \frac{1}{\Delta_J} \begin{bmatrix} -W_{i(-J)}^* W_{i(0)} \dots -W_{i(-1)}^* W_{i(0)} & \sum_{\substack{k=-J \\ k \neq 0}}^{J} \left| W_{i(k)} \right|^2 & -W_{i(1)}^* W_{i(0)} \dots & -W_{i(J)}^* W_{i(0)} \\ W_{i(-J)}^* \quad \dots \quad W_{i(-1)}^* & 0 & W_{i(1)}^* \quad \dots & W_{i(J)}^* \end{bmatrix}. \tag{B.3}$$

By substituting (B.3) in (25), expression (29) is finally obtained.

APPENDIX C

Proof of the Proposition 3

Since *NNPG* = 1 for the rectangular window, (28) becomes:

$$\mathrm{var}[\hat{B}_{e,J\,1}] = \left[(W_{e,J}^{*} W_{e,J})^{-1}\right]_{11} \frac{\sigma^2}{M}. \tag{C.1}$$

By substituting (B.2) in (C.1) we achieve:

$$\mathrm{var}[\hat{B}_{e,J\,11}] = \frac{\sigma^2}{M} \frac{1}{\Delta_J} \sum_{k=-J}^{J} \left|W_{i(k)}\right|^2. \tag{C.2}$$

According to (5) the DTFT of the rectangular window is given by:

$$W(\lambda) = \frac{\sin(\pi\lambda)}{\pi\lambda} e^{-j\pi\lambda}, \tag{C.3}$$

from which:

$$\frac{1}{\Delta_J} \sum_{k=-J}^{J} \left|W_{i(k)}\right|^2 = \frac{\sum_{k=-J}^{J} \left|W_{i(k)}\right|^2}{\sum_{\substack{k=-J \\ k\neq 0}}^{J} \left|W_{i(k)}\right|^2} = 1 + \frac{\left|W_{i(0)}\right|^2}{\sum_{\substack{k=-J \\ k\neq 0}}^{J} \left|W_{i(k)}\right|^2} = 1 + \frac{1}{\sum_{\substack{k=-J \\ k\neq 0}}^{J} \left(\frac{2l+2\delta}{2l+2\delta+k}\right)^2} \cong \frac{2J+1}{2J}. \tag{C.4}$$

where in the last equality we assume that the number of observed sine-wave cycles *l* is enough higher than *J*, while *J* is a small integer.

By substituting (C.4) in (C.2), expression (30) is finally obtained.

APPENDIX D

Proof of the Proposition 4

From (29) it follows:

$$\begin{aligned} &\left|X_{w(\delta)}\right| - \sum_{\substack{k=-J \\ k\neq 0}}^{J} \frac{\left|W(2l+2\delta+k)\right| \cdot \left|W(2l+2\delta)\right|}{\Delta_J} \cdot \left|X_{w(\delta+k)}\right| \le \left|\hat{B}_{e,J_1}\right|, \\ &\left|\hat{B}_{e,J_1}\right| \le \left|X_{w(\delta)}\right| + \sum_{\substack{k=-J \\ k\neq 0}}^{J} \frac{\left|W(2l+2\delta+k)\right| \cdot \left|W(2l+2\delta)\right|}{\Delta_J} \cdot \left|X_{w(\delta+k)}\right| \end{aligned} \tag{D.1}$$

Since the correlation coefficients between $\left|X_{w(\delta)}\right|$ and $\left|X_{w(\delta+k)}\right|$, $k = \pm1, \pm2, \ldots$, are almost nulls when the rectangular window is used [24], [25], it follows that the variances of the above lower and upper bounds and of $\left|\hat{B}_{e,J_1}\right| = \hat{A}_J / 2$ itself, coincides. By applying the law of uncertainty propagation [26] to one of the bounds above we have:

$$\mathrm{var}[\hat{A}_{e,J}] \cong 4\left(1+\frac{|W(2l+2\delta)|^2}{\Delta_J}\right)\mathrm{var}[|X_w|], \tag{D.2}$$

where $\mathrm{var}[|X_w|] \cong \sigma^2/(2M)$ is the variance of the considered DTFT samples [24], [25]. Thus, we finally obtain:

$$\mathrm{var}[\hat{A}_{e,J}] \cong \left(1+\frac{|W(2l+2\delta)|^2}{\Delta_J}\right)\cdot\frac{2\sigma^2}{M}. \tag{D.3}$$

Using (C.3) we have:

$$\frac{|W(2l+2\delta)|^2}{\Delta_J} = \frac{1}{\sum_{\substack{k=-J \\ k\neq 0}}^{J}\left(\frac{2l+2\delta}{2l+2\delta+k}\right)^2} \cong \frac{1}{2J} \tag{D.4}$$

where in the last equality we assume that the number of observed sine-wave cycles l is enough higher than J, while J is a small integer.

By substituting (D.4) in (D.3), expression (31) for $\mathrm{var}[\hat{A}_{e,J}]$ is finally obtained.

When δ is known, by substituting (31) in (13), expression (32) for $\mathrm{var}[\hat{\phi}_{e,J}]$ is achieved. When δ is estimated *a-priori* and ν is high enough that $\left|X_{w(\delta+k)}\right|$ becomes negligible, from (29) it follows that:

$$\hat{\phi}_{e,J} \cong \hat{\phi}^0_{e,J} - \pi\Delta\delta, \tag{D.7}$$

where $\hat{\phi}^0_{e,J}$ is the phase estimated under the assumption that δ is known and $\Delta\delta \overset{\Delta}{=} \hat{\delta} - \delta$ is the frequency estimation error.

By applying the law of uncertainty propagation [26] to (D.7), noticing that the correlation coefficient between $\hat{\phi}^0_{e,J}$ and $\Delta\delta$ is null because $\hat{\phi}^0_{e,J}$ is the estimates obtained when δ is known, it follows that:

$$\mathrm{var}[\hat{\phi}_{e,J}] \cong \mathrm{var}[\hat{\phi}^0_{e,J}] + \pi^2\,\mathrm{var}[\hat{\delta}], \tag{D.8}$$

where $\mathrm{var}[\hat{\phi}^0_{e,J}]$ is given by (32). By substituting (32) in (D.8) expression (33) is finally obtained.

REFERENCES

[1] IEEE Standard for Digitizing Waveform Recorders, IEEE Std. 1057-2007, 2007.

[2] IEEE Std. 1241, Standard for Terminology and Test Methods for Analog-to-Digital Converters, Dec., 2010.

[3] European Project DYNAD. Methods and Draft Standards for the Dynamic Characterization and Testing of Analog-to-Digital Converters.

[4] S.M. Kay, Fundamentals of Statistical Signal Processing: Estimation Theory, vol. 1, Upper Saddle River, NJ: Prentice-Hall, 1993.

[5] P. Händel, "Properties of the IEEE-STD-1057 four-parameter sine wave fit algorithm," *IEEE Trans. Instrum. Meas.*, vol. 49, no. 6, pp. 1189-1193, Dec. 2000.

[6] T. Andersson and P. Händel, "IEEE standard 1057, Cramér-Rao bound and the parsimony principle," *IEEE Trans. Instrum. Meas.*, vol. 55, no. 1, pp. 44-53, Feb. 2006.

[7] D. Belega, D. Petri, and D. Dallet, "Noise power estimation by the three-parameter and four-parameter sine-fit algorithms," *IEEE Trans. Instrum. Meas.*, vol. 61, no. 12, pp. 3234-3240, Jul. 2012.

[8] F.C. Alegria, "Bias of amplitude estimation using three-parameter sine fitting in the presence of additive noise," *Meas.*, vol. 42, no. 5, pp. 748-756, 2009.

[9] P. Händel, "Amplitude estimation using IEEE-std-1057 three-parameter sine wave fit: statistical distribution, bias and variance," *Meas.*, vol. 43, no. 6, pp. 766-770, 2010.

[10] D. Belega and D. Petri, "Accuracy analysis of the sine-wave parameters by means of the windowed three-parameter sine-fit algorithm," *Digital Signal Process.*, vol. 50, pp. 12-23, Mar. 2016.

[11] T.Z. Bilau, T. Megyeri, A. Sárhegyi, J. Márkus, and I. Kollár, "Four-parameter fitting of sine wave testing result: Iteration and convergence," *Comput. Stand. Interfaces*, vol. 26, no. 1, pp. 51-56, 2003.

[12] J.P. Deyst, T.M. Sounders, and O. Solomon, Jr., "Bounds on least-squares four-parameter sine-fit errors due to harmonic distortion and noise," *IEEE Trans. Instrum. Meas.*, vol. 44, no. 3, pp. 637-642, Jun. 1995.

[13] P. Carbone, E. Nunzi, and D. Petri, "Frequency-domain-based least-squares estimation of multifrequency signal parameters," *IEEE Trans. Instrum. Meas.*, vol. 49, no. 3, pp. 555-558, Jun. 2000.

[14] L-M. Zhu, H-X. Li, and H. Ding, "Estimation of multi-frequency signal parameters by frequency domain non-linear least squares," *Mech. Syst. Signal Process.*, vol. 19, pp. 955-973, 2005.

[15] D. Belega, D. Petri, and D. Dallet, "A frequency-domain linear least-squares approach for complex sine-wave amplitude and phase estimation," in Proc. IEEE I2MTC Conference, Torino, Italy, May 22-25, 2017.

[16] A.H. Nuttall, "Some windows with very good sidelobe behavior," *IEEE Trans. Acoust., Speech, Signal Processing*, vol. ASSP-29, no.1, pp 84–91, Feb. 1981.

[17] D. Belega and D. Dallet, "Multifrequency signal analysis by interpolated DFT method with maximum sidelobe decay windows," *Measurement*, vol. 42, no. 3, pp. 420-426, Apr. 2009.

[18] F.J. Harris, "On the use of windows for harmonic analysis with the discrete Fourier transform," *Proc. of the IEEE*, vol. 66, no. 1, pp. 51–83, Jan. 1978.

[19] C. Offelli and D. Petri, “The influence of windowing on the accuracy of multifrequency signal parameter estimation,” *IEEE Trans. Instrum. Meas.*, vol. 41, no. 2, pp. 256-261, Apr.1992.

[20] C. Offelli and D. Petri, “Interpolation techniques for real-time multifrequency waveform analysis,” *IEEE Trans. Instrum. Meas.*, vol. 39, no. 1, pp. 106-111, Feb. 1990.

[21] E. Aboutanios and B. Mulgrew, “Iterative frequency estimation by interpolation on Fourier coefficients,” *IEEE Trans. Signal Process.*, vol. 53, no. 4, pp. 1237-1241, Apr. 2005.

[22] D. Belega, D. Petri, and D. Dallet, “Iterative sine-wave frequency estimation by generalized Fourier interpolation algorithms,” in Proc. 11th IEEE ISETC 2014 symposium, pp. 105-108, November 14-15, 2014, Timişoara, Romania.

[23] D. Belega, D. Petri, and D. Dallet, “Accuracy of sine-wave frequency estimation by an iterative interpolated DFT algorithm,” in Proc. I2MTC conference, pp. 1795-1800, May 11-14, 2015, Pisa, Italy.

[24] C. Offelli and D. Petri, “Weigthing effect on the dicrete time Fourier transform of noisy signals,” *IEEE Trans. Instrum. Meas.*, vol. 40, no. 6, pp. 972-981, Dec. 1991.

[25] M. Novotný, D. Slepička, and M. Sedláček, “Uncertainty analysis of the RMS value and phase in frequency domain by noncoherent sampling,” *IEEE Trans. Instrum. Meas.*, vol. 56, no. 3, pp. 983-989, May 2007.

[26] Guide for the expression of uncertainty in measurement (GUM), International Organization for Standardization, Switzerland, second edition, 1995.